Effects of alloying elements on twinning in Ni-based superalloys

Valery V. Borovikov[1, *], Mikhail I. Mendelev[2], Timothy M. Smith[3], John W. Lawson[2]

[1]KBR, Inc., Intelligent Systems Division, NASA Ames Research Center, Moffett Field, CA 94035, USA
[2]Intelligent Systems Division, NASA Ames Research Center, Moffett Field, CA 94035, USA
[3]NASA Glenn Research Center, Cleveland, OH 44135, USA

Abstract

Micro-twinning is the major creep deformation mechanism in Ni-based superalloys at temperatures above 700 °C. Recent experiments suggest that superlattice stacking faults in γ′ phase may serve as the precursors to twin formation. Segregation of alloying elements to these precursors may have a significant effect on formation and extension of micro-twins. Using atomistic modeling we investigate and explain the effects of Nb and Cr alloying additions on these processes. The simulation shows that Nb increases the creep resistance which is mostly associated with impeding the reordering of the high energy double complex stacking fault. Cr, on the other hand, promotes twin growth, degrading the high temperature creep properties. These results can help to understand the effects of elemental composition of the alloy on creep resistance.

* Corresponding author: valery.v.borovikov@nasa.gov

1. Introduction

Ni-based superalloys are widely used in the hot sections of aircraft turbine engines because of their exceptional creep resistance at high temperatures. This creep resistance is associated with the presence of the γ′ precipitates coherently embedded in the matrix, γ, which is face-centered cubic (fcc) solid solution. A single dislocation penetrating a γ′ precipitate necessarily creates a stacking fault with an energy much higher than that in the γ matrix. However, the situation becomes much more complex when several dislocations traveling on adjacent planes approach a γ′ precipitate. For example, in the mechanism originally proposed by Kolbe [1], a high energy double complex stacking fault (CSF), created by the pairs of 1/6⟨112⟩ partial dislocations moving on adjacent {111} glide planes can transform into a lower energy superlattice extrinsic stacking fault (SESF) via thermally activated reshuffling [2]. Recent experiments suggest that superlattice stacking faults in γ′ phase may serve as the precursors to twin formation, which is one of the major deformation mechanisms in Ni superalloys at intermediate temperatures (600 °C – 800 °C) [3]. Segregation of alloying elements to these precursors may have a significant effect on formation and extension of micro-twins. In particular, segregation of γ phase formers (e.g., Co, Cr) at superlattice intrinsic stacking faults (SISF), SESF and twin interfaces within γ′ phase have been observed experimentally to contribute to faster creep strain rates. Many studies have reported that this γ softening effect may make alloys more susceptible to micro-twinning under creep deformation conditions, thus significantly increasing creep deformation [4-6]. Conversely, recent research has found that alloys with increased concentrations of Nb and Ta, were less likely to develop twins under creep deformation conditions by inhibiting the γ softening effect.

In this study, we explore the effects of alloying elements on twin formation and growth in Ni-based superalloys. Employing recently developed simulation methodology [2] along with Finnis-Sinclair (FS) potentials for Ni-Al-Nb [8] and Ni-Al-Cr [9], specifically developed for this study, we investigate the effects of Nb and Cr on deformation twinning in Ni superalloys.

2. Simulation geometry and procedure

All simulations were carried out using the LAMMPS package [10]. Recently developed Finnis-Sinclair (FS) [11] potentials for Ni-Al [12], Ni-Al-Nb [8] and Ni-Al-Cr [9] were used to describe the interaction between atoms in a binary Ni-Al alloy and in ternary Ni-Al-Nb and Ni-Al-Cr alloys, correspondingly. A composite system, used in our simulations, contained γ phase (matrix) and γ′ phase (precipitate) regions and two edge dislocation dipoles (see Fig. 1a). The dipoles were positioned such that individual dislocations of the upper and lower dislocation pairs would glide on the adjacent {111} planes when a σ_{xz} shear stress was applied. The system size was: ~100×2.5×29 nm^3 and contained ~700,000 atoms. As constructed, the model contained ~12.5% of Al in the γ matrix (solid solution of Al in fcc Ni), while the region of the γ′ precipitate corresponded to perfect $L1_2$ (Ni_3Al) lattice. Prior to the introduction of the dipoles into the simulation cell, a hybrid Monte Carlo / molecular dynamics (MC/MD) relaxation was performed at T = 1300 K and zero applied stress, using periodic boundary conditions (PBCs) in all directions. The details of the MC/MD relaxation procedure were as follows: every 50 MD steps the simulation was interrupted to perform MC trial exchange events (swaps of Al with Ni) for 5% randomly chosen Al atoms. Every Al atom was subjected to ~750 trial exchanges during the entire MC/MD relaxation course.

As a result, the γ/γ' interfaces became less sharp, and a small number of anti-site defects (Ni substituting Al in $L1_2$) was formed in the precipitate region. Following the MC/MD relaxation procedure, two edge dislocation dipoles were introduced into the matrix region of the simulation cell (see Fig. 1a). Details of the dislocation dipole construction can be found in Refs. [13, 14]. To facilitate thermally activated diffusion, 350 vacancies were introduced into the simulation model, corresponding to a vacancy concentration of 0.05%. Such a high vacancy concentration (along with the elevated simulation temperature) was needed to simulate the thermally activated reordering processes on the time scale of MD simulation. The deformation simulations were carried out at T = 1300 K under the following combined applied shear stresses: σ_{xz} = 600 MPa, σ_{yz} = -1039 MPa. The shear stresses were gradually ramped up from zero to the target values during the time interval of 80 ps. The rest of the stress components were kept zero using a barostat. After reaching the target stress values, the system was kept under these constant shear stresses for the rest of the simulation. Application of σ_{yz} was necessary to decouple the $1/2\langle 110\rangle$ dislocations (the resulting $\sigma_{xz} + \sigma_{yz}$ stress provides zero driving force for the trailing $1/6\langle 112\rangle$ partial dislocations) [15, 16]. As a result, the dislocations dissociate and only the leading $1/6\langle 112\rangle$ partials penetrate the γ' precipitate when the pairs of like sign dislocations, travelling on the adjacent {111} slip planes, arrive to the opposite sides of the precipitate (see Fig. 1b).

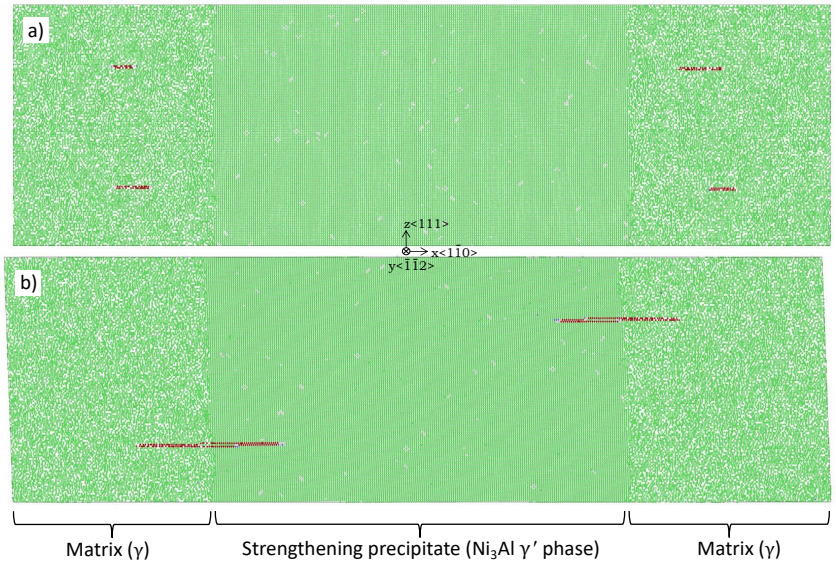

Fig. 1: Simulation system. a) In the beginning of the simulation. b) In the course of the MD deformation simulation. Ni atoms are not shown. Colored according to Common Neighbor Analysis (CNA). Green – fcc, red – hcp, grey – other.

3. Binary Ni-Al system

The authors of the present study recently investigated the Kolbe micro-twinning mechanism employing atomistic simulations [2]. It was demonstrated that atomic diffusion-mediated reordering takes place in the immediate vicinity of the cores of twinning partials and proceeds in a highly concerted manner, directly influenced by propagation of the dislocations (see Fig. 2). The first partial (in each pair) entering inside the precipitate produces a complex stacking fault (CSF) which is energetically unfavorable (Al-Al nearest neighbor bonds (NNBs) are created). As

discussed in detail in Ref. [2], the second leading partial, gliding on the adjacent {111} plane, generates the high energy Al-Al-Al NNBs sequentially, one after another, along [1 0 -1] direction, as it glides from the left to the right inside the strengthening precipitate (see Fig. 2). In the Kolbe mechanism, the system's response to this generation of the high energy atomic configurations is the reshuffling, which as was shown in Ref. [2], follow the same sequence, because each consecutive reshuffling move triggers the next one in the sequence: after completion of one reshuffling event, the next Al atom which is going to swap with Ni along the row, receives an extra Al bond (on top of the two NNBs already produced by the glide of the partials), that provides an extra driving force (assistance) to execute the reshuffling move (see Fig. 2b and Ref. [2]).

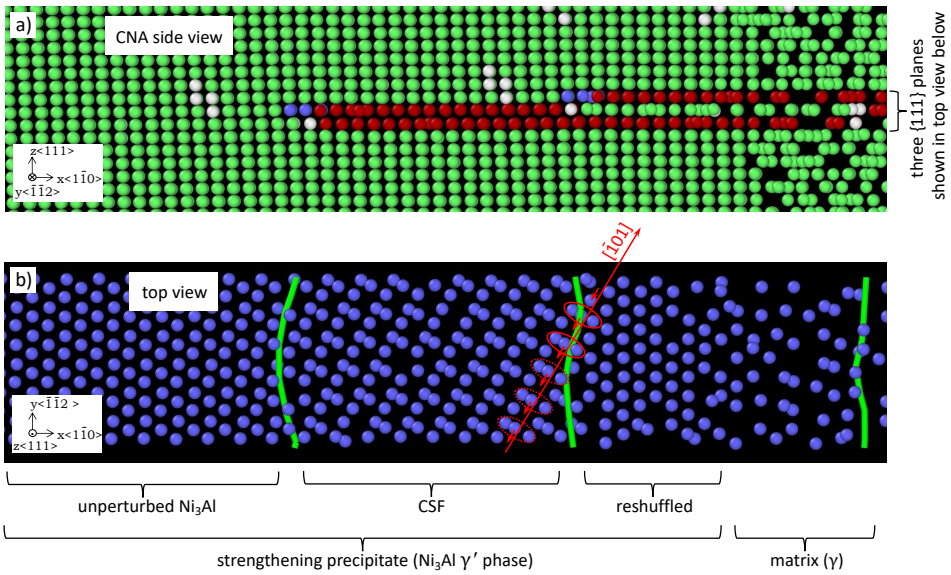

Fig. 2: Propagation of the pair of partial dislocations (on adjacent {111} glide planes) inside the strengthening precipitate (Ni-Al system) [2]. Ni atoms are not shown. a) Side view. Colored according to CNA (green – fcc, red – hexagonal close-packed (hcp)). b) Top view of the same atomic configuration demonstrates the process of sequential creation of triple Al-Al NNs (highlighted by red ovals) and the consecutive reordering moves (indicated by small red arrows): each move triggers the next one in the sequence. Partial dislocations are highlighted in green.

4. Alloying with Nb

In order to simulate the effect of Nb, we took the simulation cell described in Section 2 (prior to introduction the dislocation dipoles) and replaced ~3% of Al atoms by Nb. Then the MC/MD was performed again. In this case, every 50 MD steps the simulation was interrupted to perform MC trial exchange events (swaps of Nb with Ni and Al) for 5% randomly chosen Nb atoms. Every Nb atom was subjected to ~1000 trial exchanges during the MC/MD relaxation. The distribution of Nb atoms after MC/MD relaxation is shown in Fig. 3. As can be seen, the most of Nb atoms reside inside γ′ phase strengthening precipitate.

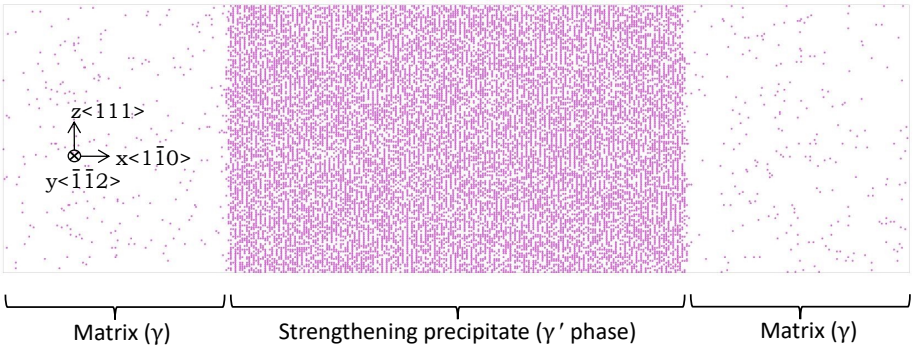

Fig. 3: Distribution of Nb atoms (Ni and Al atoms are not shown).

Following the MC/MD relaxation procedure, two edge dislocation dipoles were introduced into the matrix region of the simulation system. Using the same applied stresses, as described in Section 2 for pure Ni-Al system, we carried out the deformation simulation at T=1300K. Relatively small Nb addition (~3 at.%) we used in this study, significantly slowed down the reordering processes. Fig. 4 compares the progress in two systems (with and without Nb) at about the same level of deformation. We can see that the double CSF behind the partial traveling on the upper {111} plane in pure Ni-Al system is completely reshuffled (see Fig. 4a). On the other hand, in the system with Nb, the double CSF is only partially reshuffled (see Fig. 4b). Since the reshuffling is the rate limiting process, which reduces the energy of the defect generated inside the strengthening precipitate by the glide of the coupled partial dislocations, the dislocations in the system with Nb cannot propagate any further inside the precipitate until the most of the high energy configurations that include Al and Nb atoms (highlighted by the red ovals in Fig. 4) have been eliminated. This requires more time, and, as a result in the system with Nb deformation creep is progressing much slower, compared to the pure Ni-Al system.

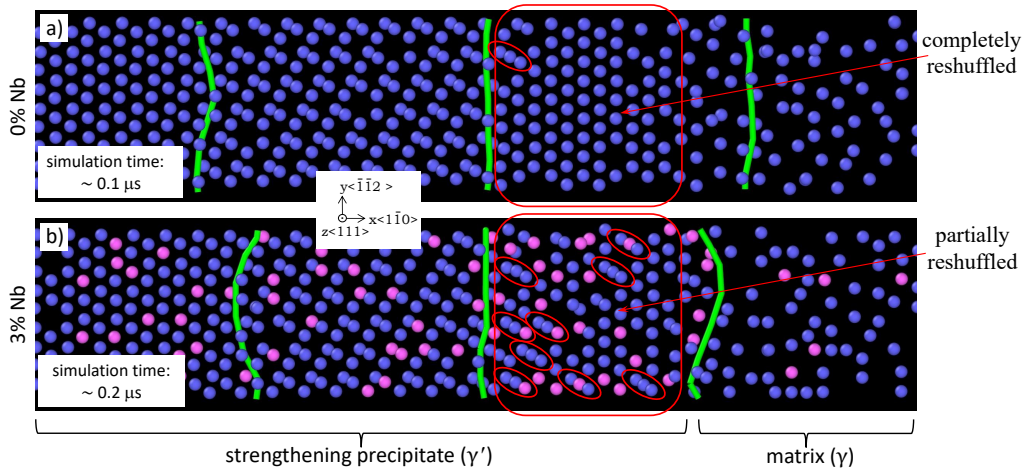

Fig. 4: Effect of Nb solute addition on reshuffling processes. T=1300K. a) pure Ni-Al system (*simulation time* ~ *0.1 μs*). The double CSF generated by the partial dislocations is completely reordered. b) The system with ~ 3% Nb (*simulation time* ~ *0.2 μs*). The reordering of the double CSF is incomplete. High energy configurations that include Al and Nb atoms are highlighted by red ovals. Ni atoms are not shown. Nb atoms are highlighted in pink. Partial dislocations are highlighted in green.

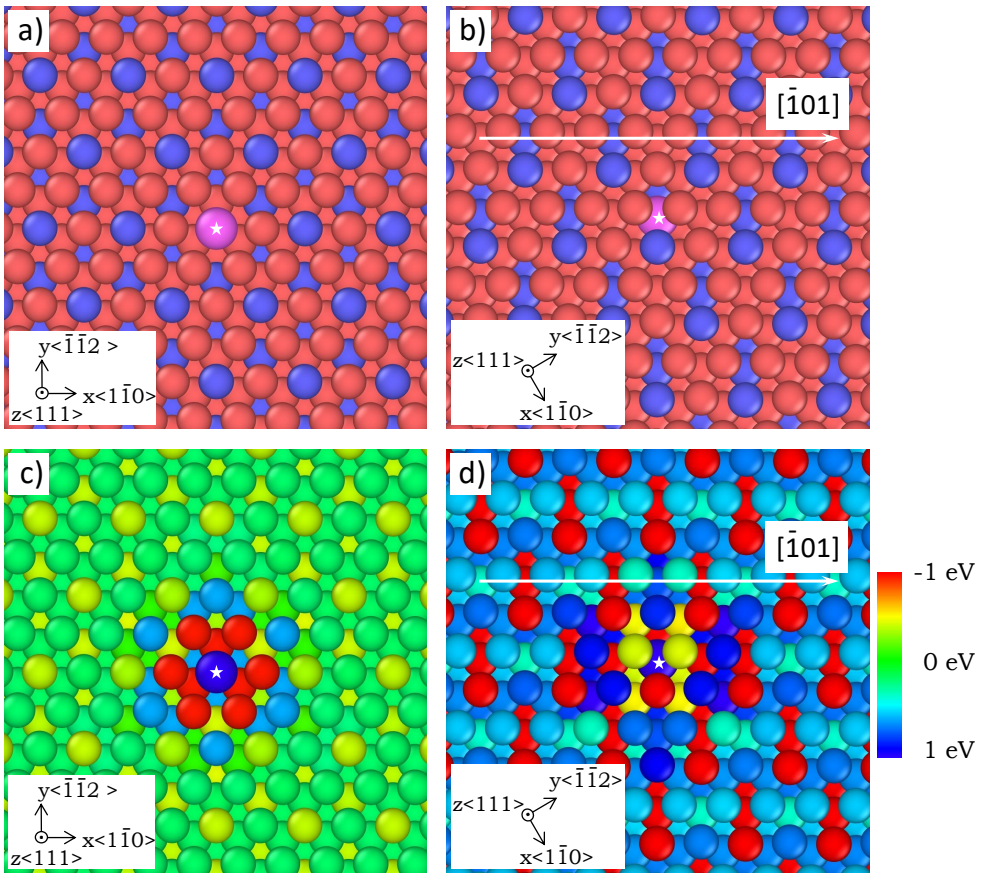

Fig. 5: Local stress field due to Nb atom (highlighted by the small star in all images). a) and c) show Nb atom in bulk $L1_2$. b) and d) show Nb atom at double CSF. a) and b) are colored according to atom type: red – Ni, blue – Al, pink – Nb. c) and d) are colored according to the trace of the atomic stresses multiplied by the average atomic volume in the simulation cell.

Stiffer Nb atoms, substituting Al atoms in $L1_2$, introduce appreciable local stress fields (see Fig. 5). Interaction between the stress fields of the dislocations and the stress fields induced by Nb solutes is another reason for the slower dislocation propagation in the system with Nb solutes, compared with pure Ni-Al system. As already mentioned, it was expected that sluggish diffusing Nb atoms would slow down the speed of reordering in situations when Nb atoms must move, in order to eliminate the NNBs with Al, or Nb atoms. Surprisingly, we observe that Nb atoms also slow down reshuffling of nearby Al-Al-Al nearest neighbor configurations (see Fig. 4). This effect could be due to the local stress fields induced by Nb atoms and their stiffness (see Figs. 5c, 5d).

5. Semi-empirical potential

In order to compare the effects of Nb and Cr we need to have a set of consistent semi-empirical potentials. Since the study of the effect of Nb was performed using the FS potential from [8] in the present study, we developed an FS potential for Ni-Al-Cr where the Ni-Al part was taken from [8, 12]. The potential energy in the FS approach takes the following form:

$$U = \sum_{i=1}^{N-1} \sum_{j=i+1}^{N} \varphi^{t_i t_j}(r_{ij}) + \sum_{i=1}^{N} \Phi^{t_i}(\rho_i), \quad (1)$$

where t_i is the atom i type, N is the number of atoms, r_{ij} is atomic separation, $\varphi^{t_i t_j}(r)$ is the pair potential, $\Phi^{t_i}(\rho_i)$ is the embedding energy function,

$$\rho_i = \sum_{\substack{j=1 \\ j \neq i}}^{N} \psi^{t_i t_j}(r_{ij}) \quad (2)$$

is the "electron" density which is assumed to be a sum of pair contributions, $\psi^{t_i t_j}(r)$. In order to add Cr to an existing Ni-Al potential, one should develop an FS potential for pure Cr and fit 2 cross pair potentials (Ni-Cr and Al-Cr) and 2 cross-density functions.

In the case of pure Cr, we mostly used experimental data as the target values (see Table I) in the potential development procedure supplementing them with *ab initio* data only when experimental data were not available. The only exception was the lattice parameter for the bcc Cr at T=0 which was taken from the *ab initio* calculations. This was associated with the fact that the *ab initio* calculations with the with PBEsol exchange-correlation functional [17] used in the present study tend to overestimate the atomic density and since the liquid structure data were taken from the *ab initio* molecular dynamics (AIMD) simulation we had to use the "*ab initio*" density everywhere for the sake of self-consistency of the target values.

In the case of Cr solution in the Ni-Al alloys we used only *ab initio* data as the target values in the potential development procedure. The main problem here is associated with the fact that Cr can occupy both Ni and Al sites in the γ′ phase. Therefore, the properties of both Cr_3Al and Ni_3Cr compounds were included because in the former case, Cr resides on Ni sites while in the latter case Cr resides on Al sites. Finally, the potential was fit to the experimental data on Cr partitioning between the γ and γ′ phases.

In order to get the target *ab initio* data, we used the Vienna Ab initio Simulation Package (VASP) with PBEsol exchange-correlation functional [18, 19]. The Monkhorst-Pack Γ- centered k-mesh was used for the Brillouin zone integration [20]. The charge self-consistency convergence was accelerated using the modified Broyden's method [21]. The plane-wave energy cutoff (ENCUT) was increased to 650 eV. Collinear spin-polarized calculations (ISPIN=2) were performed for magnetic systems, such as nickel. Formation energies were computed relative to the energies of elemental solids in their ground states [22].

The potential development procedure used in the present study was described in Ref. [23]. Two features of this procedure should be emphasized. The first one is concurrent fitting the potential functions for pure Cr and cross-functions. This feature allows to better reproduce the alloy properties in expense of the pure Cr properties and clearly makes sense for the present study where the focus was the effect of Cr on the creep properties of Ni-Al alloys rather than the properties of pure Cr [24]. This is why the agreement with target values listed in Table I is somewhat worse than one could expect from the state-of-the-art FS potential for a pure metal (e.g., see [24]). Especially, one can notice a poor agreement for the cohesive energy and the bcc-fcc energy difference. However, the cohesive energy itself is directly relevant for simulation of processes like sublimation, which was obviously not the focus of the present study and the bcc Cr phase never appears in our MD simulation. On the other hand, the potential correctly reproduces the Cr lattice parameter making its atomic radius larger than that for Ni and smaller than that for Al which should be very relevant to the question on which sites in the γ′ phase Cr prefers to reside. The potential also well reproduces the Cr melting temperature which is directly related to its atomic stiffness.

Examination of Tables II and III shows that the developed potential provides a reasonable agreement with the *ab initio* $L1_2$ lattice parameters for both Cr_3Al and Ni_3Cr phases which is important for the lattice mismatch between the γ and γ′ phases. The formation energies are not well reproduced, but these quantities include the properties of the alloy and pure elements such that they may not be very relevant to the scope of the present study. On the other hand, the developed potential correctly reproduces the fact that all competing Ni_3Cr phases listed in Table II except of $D0_3$ have about the same energies. At the same time, the developed potential also reproduces the fact that the Cr_3Al $L1_2$ phase has a higher energy than do the other competing Cr_3Al phases. This fact may correlate with the Cr preference to reside on the Al sites over residing on the Ni sites.

Finally, the semi-empirical potential was fit to reproduce the fact that the most of Cr atoms reside in the γ phase. To check that the potential indeed reproduces the experimentally observed partitioning of Cr we randomly replaced ~30% of atoms (Ni and Al) by Cr in the matrix region of the simulation cell described in Section 2 (the simulation cell did not contain dislocation dipoles) and performed MC/MD relaxation T = 1000 K and zero applied stress. The details of the MC/MD relaxation procedure were as follows: every 50 MD steps the simulation was interrupted to perform MC trial exchange events (swaps of Cr with Ni and Al) for 5% randomly chosen Cr atoms. Every Cr atom was subjected to ~1000 trial exchanges during the MC/MD relaxation. The distribution of Cr atoms after MC/MD relaxation is shown in Fig. 6. As can be seen, most of Cr atoms reside inside γ phase, however, there is a considerable amount of Cr in the γ′ phase where it resides on both Al and Ni sites.

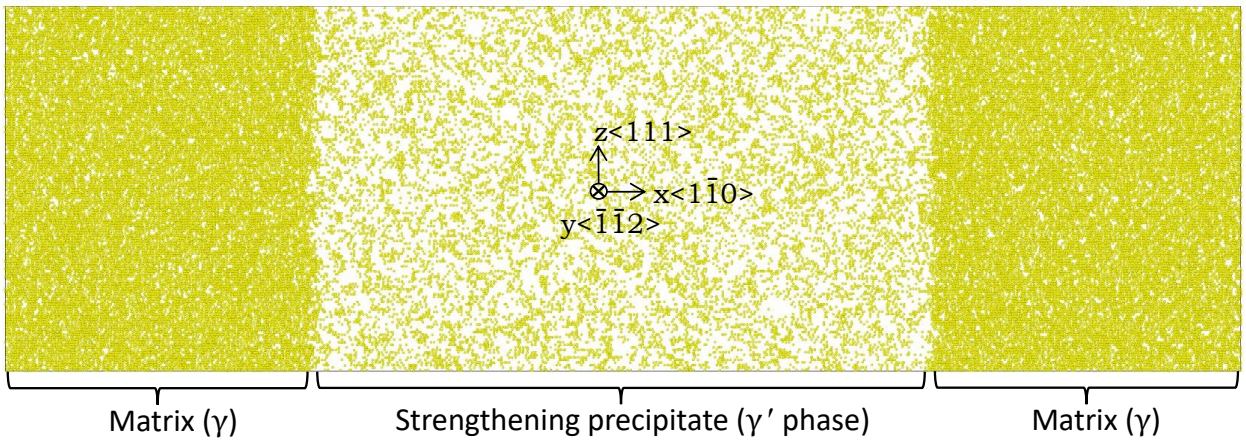

Fig. 6: Distribution of Cr (Ni and Al atoms are not shown).

Table I. The properties of pure Cr[ε]

Property	Target value	FS potential
a (bcc) (Å)	2.812€	**2.813**
E_{coh} (bcc) (eV/atom)	-4.1[§]	**-7.5**
C_{11} (GPa)	411[§]	**416**
C_{12} (GPa)	107[§]	**100**
C_{44} (GPa)	105[§]	**171**
E_f^v (relaxed bcc) (eV/atom)	1.8[§]	**1.52**
E_m^v (bcc) (eV/atom)	1.3[§]	1.06
E_D (bcc) (eV/atom)	3.1[§]	2.58
$\Delta E_{fcc\rightarrow bcc}$ (eV/atom)	0.075[£]	**0.296**
T_m (bcc) (K)	2163[¥]	2168
ΔH_m (bcc, T_m) (eV/atom)	0.218[¥]	**0.225**
$\Delta V_m/V_s$ (bcc, T_m) (%)		5.9

Table II. properties of Ni_3Cr phases at T=0.

Property	Target value[€]	FS potential
a ($L1_2$) (Å)	3.495	**3.486**
ΔE_f ($L1_2$) (eV/atom)	-0.001	**0.117**
$\Delta E_{L1_2\rightarrow D0_{19}}$ (eV/atom)	0.003	**-0.038**
$\Delta E_{L1_2\rightarrow D0_{22}}$ (eV/atom)	-0.022	**-0.076**
$\Delta E_{L1_2\rightarrow D0_{23}}$ (eV/atom)	0.002	**-0.036**
$\Delta E_{L1_2\rightarrow D0_{24}}$ (eV/atom)	-0.003	**-0.015**
$\Delta E_{L1_2\rightarrow D0_3}$ (eV/atom)	0.116	**0.122**

Table III. properties of Cr_3Al phases at T=0.

Property	Target value[€]	FS potential
a ($L1_2$) (Å)	3.632	**3.627**
ΔE_f ($L1_2$) (eV/atom)	0.186	**-0.068**
$\Delta E_{L1_2\rightarrow D0_{19}}$ (eV/atom)	-0.088	**-0.106**
$\Delta E_{L1_2\rightarrow D0_{22}}$ (eV/atom)	-0.034	**0.024**
$\Delta E_{L1_2\rightarrow D0_{23}}$ (eV/atom)	-0.024	**-0.024**
$\Delta E_{L1_2\rightarrow D0_{24}}$ (eV/atom)	-0.048	**-0.063**
$\Delta E_{L1_2\rightarrow D0_3}$ (eV/atom)	-0.110	**-0.276**
$\Delta E_{L1_2\rightarrow Pm\bar{3}n}$ (eV/atom)	-0.266	**-0.086**

[ε] The properties used in the fitting procedure are printed in bold.
[€] *Ab initio* calculation performed in the present study.
[§] B. J. Lee, M. I. Baskes, H. Kim, and Y. K. Cho, Physical Review B 64, 184102 (2001).
[£] J. E. Saal, S. Kirklin, M. Aykol, B. Meredig, and C. Wolverton, JOM **65,** 1501 (2013).
[¥] A. I. Efimov, L. P. Belorukova, and I. V. Vasilkova, (Himiia, Leningrad, 1983), Svoistva neorganicheskikh soedinenii. Spravochnik.

6. Alloying with Cr

According to the experimental observations, Cr occupies Al-sites of Ni_3Al-based γ' strengthening precipitates (both, in the bulk, and in the elemental segregated regions near fault) of ME3, etc [26]. On the other hand, the results of DFT calculations performed to determine the interaction energies between Cr solutes and stable stacking faults in γ'-Ni_3Al indicate that Cr (on Al sublattice) is repelled from these faults [25]. The DFT-informed interatomic simulation potential for Ni-Al-Cr, used in this study, also yields positive interaction energies between Cr solute and stable stacking faults in γ'-Ni_3Al. So, employing this potential does not reproduce the experimentally observed segregation of Cr at stacking faults. A follow-up DFT study (see Ref. [27]) explained the experimentally observed segregation of Cr to the stacking faults in γ'-Ni_3Al by the effects of co-segregation of Cr and Co. It was demonstrated that segregation of Co on the Ni sublattice at the fault draws segregation of Cr that has a positive segregation enthalpy at the fault without the presence of Co [27]. Since the interatomic simulation potential for the quaternary Ni-Al-Co-Cr system is currently not available, we manually created the regions with 6% Cr concentration (following the experimental observations [26], Cr atoms were placed on Al sites) in the Ni-Al simulation cell described in Section 2, in order to study the associated effects on functionality of the Kolbe mechanism for micro-twinning (see Fig. 7). The rest of the simulation setup (simulation temperature, applied stresses, number of vacancies, etc.) was the same as the one described in Section 2.

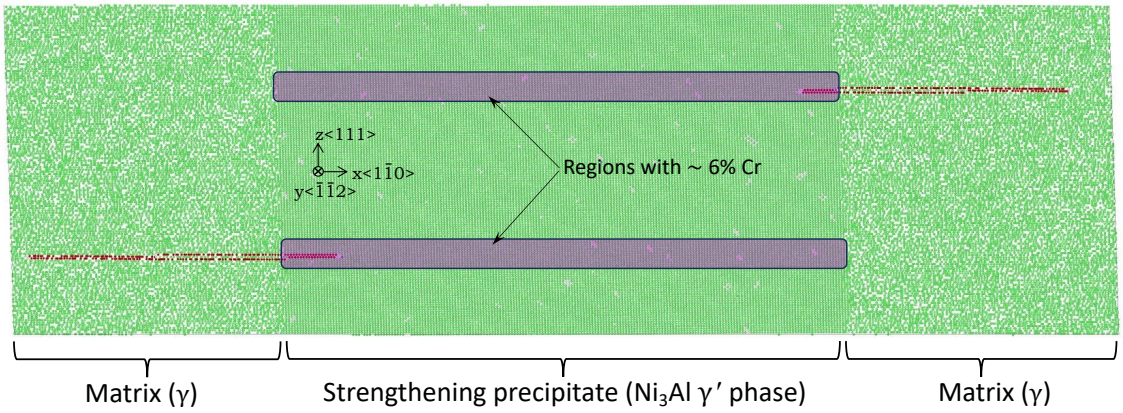

Fig. 7: Introduction of Cr into the simulation system (the regions with high Cr concentration inside the precipitate are highlighted).

Figure 8 shows a comparison of the dislocation propagation in the original Ni-Al alloy and the alloy doped with Cr (same deformation conditions were used in both cases; simulation time t = 0.1μs). Examination of this figure suggests that Cr (occupying Al sites in γ' precipitates) significantly accelerates deformation. This can be rationalized as follows. Due to non-uniform distribution of Cr, patches of γ phase are produced near preexisting stacking faults, or twin interfaces. As a result, dislocations "fly" through those patches, significantly accelerating creep.

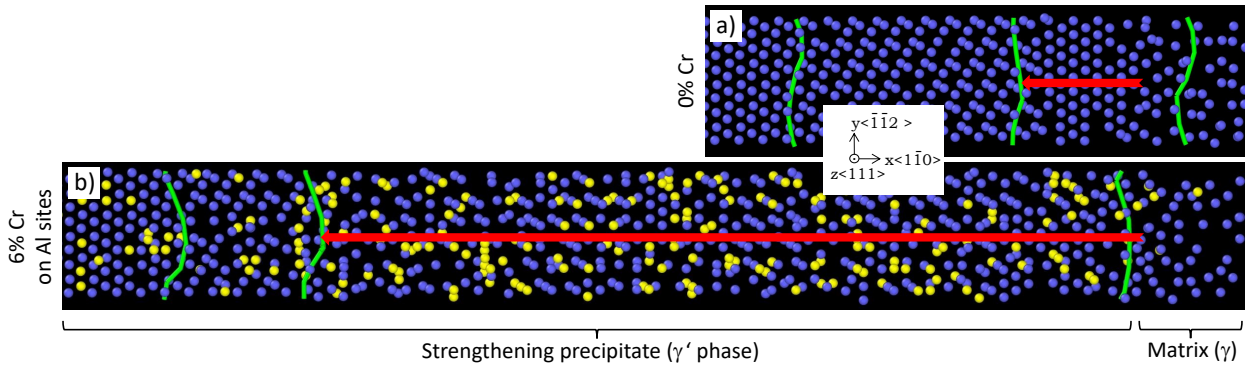

Fig. 8: Effects of Cr on high temperature deformation creep. T=1300K. Simulation time: t = 0.1μs. a) pure Ni-Al system, b) the system where ~6% Cr was introduced on Al sites. Ni atoms are not shown. Cr atoms are highlighted in yellow. Partial dislocations are highlighted in green. The red arrows schematically indicate the penetration depth of the partial that generates double CSF inside the strengthening precipitate.

7. Conclusions

Using atomistic simulations, we investigated the effects of Nb and Cr alloying additions on high temperature deformation creep properties of Ni-based superalloys. We show that relatively small addition of Nb can significantly improve the creep properties. The effect of Nb atoms is multifold. Increase in the CSF energy due to Nb atoms makes it more difficult for the dislocations to enter the strengthening precipitate (and move inside it). The glide of the dislocations is affected by the interaction with the local stress fields induced by Nb atoms. And, more importantly, the slow diffusing Nb atoms impede the reordering of the high energy double CSF. The Cr (on Al sites in γ' precipitates), on the other hand, significantly degrades the high temperature creep properties. The effect of Cr can be amplified by increased segregation of Cr at superlattice intrinsic stacking faults in γ' phase precipitates. These results can help to understand the effect(s) of elemental composition of the alloy on creep resistance.

Acknowledgements

Funding is acknowledged from the NASA Aeronautics Research Mission Directorate's (ARMD) Transformational Tools and Technologies (TTT) Project. Resources supporting this work were provided by the NASA High-End Computing (HEC) Program through the NASA Advanced Supercomputing (NAS) Division at Ames Research Center.

References

[1] M. Kolbe, The high temperature decrease of the critical resolved shear stress in nickel-base superalloys, Materials Science and Engineering: A 319 (2001) 383-387.
[2] V.V. Borovikov, M.I. Mendelev, T.M. Smith, J.W. Lawson, Dislocation-assisted diffusion-mediated atomic reshuffling in the Kolbe mechanism for micro-twinning in Ni-based superalloys from molecular dynamics simulation, Scripta Materialia 232 (2023) 115475.
[3] T.M. Smith, R.R. Unocic, H. Deutchman, M.J. Mills, Creep deformation mechanism mapping in nickel base disk superalloys, Materials at High Temperatures 33(4-5) (2016) 372-383.
[4] T. Smith, B. Esser, N. Antolin, A. Carlsson, R. Williams, A. Wessman, T. Hanlon, H. Fraser, W. Windl, D. McComb, Phase transformation strengthening of high-temperature superalloys, Nature communications 7(1) (2016) 1-7.
[5] T.M. Smith, B. Good, T. Gabb, B. Esser, A. Egan, L. Evans, D. McComb, M. Mills, Effect of stacking fault segregation and local phase transformations on creep strength in Ni-base superalloys, Acta Materialia 172 (2019) 55-65.
[6] T. Smith, T. Gabb, K. Wertz, J. Stuckner, L. Evans, A. Egan, M. Mills, Enhancing the creep strength of next-generation disk superalloys via local phase transformation strengthening, Superalloys 2020: Proceedings of the 14th International Symposium on Superalloys, Springer, 2020, pp. 726-736.
[7] A.J. Egan, F. Xue, Y. Rao, G. Sparks, E. Marquis, M. Ghazisaeidi, S. Tin, M.J. Mills, Local Phase Transformation Strengthening at Microtwin Boundaries in Nickel-Based Superalloys, Acta Materialia 238 (2022) 118206.
[8] FS potential for Ni-Al-Nb, https://www.ctcms.nist.gov/potentials.
[9] FS potential for Ni-Al-Cr, https://www.ctcms.nist.gov/potentials.
[10] S. Plimpton, Fast parallel algorithms for short-range molecular dynamics, Journal of computational physics 117(1) (1995) 1-19.
[11] M. Finnis, J. Sinclair, A simple empirical N-body potential for transition metals, Philosophical Magazine A 50(1) (1984) 45-55.
[12] FS potential for Ni-Al, https://www.ctcms.nist.gov/potentials.
[13] E. Oren, E. Yahel, G. Makov, Dislocation kinematics: a molecular dynamics study in Cu, Modelling and Simulation in Materials Science and Engineering 25(2) (2016) 025002.
[14] V.V. Borovikov, M.I. Mendelev, T.M. Smith, J.W. Lawson, Molecular dynamics simulation of twin nucleation and growth in Ni-based superalloys, International Journal of Plasticity (2023) 103645.
[15] I.J. Beyerlein, X. Zhang, A. Misra, Growth twins and deformation twins in metals, Annual Review of Materials Research 44 (2014) 329-363.
[16] R.R. Unocic, N. Zhou, L. Kovarik, C. Shen, Y. Wang, M.J. Mills, Dislocation decorrelation and relationship to deformation microtwins during creep of a γ′ precipitate strengthened Ni-based superalloy, Acta Materialia 59(19) (2011) 7325-7339.
[17] J.P. Perdew, A. Ruzsinszky, G.I. Csonka, O.A. Vydrov, G.E. Scuseria, L.A. Constantin, X. Zhou, K. Burke, Restoring the density-gradient expansion for exchange in solids and surfaces, Physical review letters 100(13) (2008) 136406.
[18] G. Kresse, J. Hafner, Ab initio molecular dynamics for liquid metals, Physical review B 47(1) (1993) 558.
[19] G. Kresse, J. Hafner, Ab initio molecular-dynamics simulation of the liquid-metal–amorphous-semiconductor transition in germanium, Physical Review B 49(20) (1994) 14251.

[20] H.J. Monkhorst, J.D. Pack, Special points for Brillouin-zone integrations, Physical review B 13(12) (1976) 5188.
[21] D.D. Johnson, Modified Broyden's method for accelerating convergence in self-consistent calculations, Physical Review B 38(18) (1988) 12807.
[22] N. Zarkevich, Structural database for reducing cost in materials design and complexity of multiscale computations, Complexity 11(4) (2006) 36-42.
[23] Y. Zhang, R. Ashcraft, M. Mendelev, C. Wang, K. Kelton, Experimental and molecular dynamics simulation study of structure of liquid and amorphous Ni62Nb38 alloy, The Journal of chemical physics 145(20) (2016).
[24] M. Mendelev, M. Kramer, C.A. Becker, M. Asta, Analysis of semi-empirical interatomic potentials appropriate for simulation of crystalline and liquid Al and Cu, Philosophical Magazine 88(12) (2008) 1723-1750.
[25] Y. Rao, T. Smith, M. Mills, M. Ghazisaeidi, Segregation of alloying elements to planar faults in γ'-Ni3Al, Acta Materialia 148 (2018) 173-184.
[26] T.M. Smith, N.A. Zarkevich, A.J. Egan, J. Stuckner, T.P. Gabb, J.W. Lawson, M.J. Mills, Utilizing local phase transformation strengthening for nickel-base superalloys, Communications Materials 2(1) (2021) 106.
[27] L. Feng, Y. Rao, M. Ghazisaeidi, M.J. Mills, Y. Wang, Quantitative prediction of Suzuki segregation at stacking faults of the γ'phase in Ni-base superalloys, Acta Materialia 200 (2020) 223-235.